Research Square

Preprints are preliminary reports that have not undergone peer review.
They should not be considered conclusive, used to inform clinical practice,
or referenced by the media as validated information.

Machine Learning-Assisted Processing Maps for Selective Laser Melted AlSi10Mg Alloy Optimization

Brajesh Parashar
Cambridge Institute of Technology
Sudha Joseph
Cambridge Institute of Technology
Shiralgi Yallappa
yallappashiralgi5@gmail.com
Cambridge Institute of Technology https://orcid.org/0000-0002-5252-5541
Sana Ben Moussa
King Khalid University
Joseph Kavitha
Cambridge Institute of Technology
Nur Insyirah Mohd Nadzri
UniMAP: Universiti Malaysia Perlis
Abdullah Yahya Abdullah Alzahrani
King Khalid University

Research Article

Keywords: Additive manufacturing, AlSi10Mg, machine learning, process optimization, selective laser sintering, property prediction

Posted Date: November 13th, 2026

DOI: https://doi.org/10.21203/rs.3.rs-11389448/v1

License: This work is licensed under a Creative Commons Attribution 4.0 International License.
Read Full License

Machine Learning-Assisted Processing Maps for Selective Laser Melted AlSi10Mg Alloy Optimization

Brajesh Parashar[1] · Sudha Joseph[1, 2*] · Shiralgi Yallappa[1, 3*] · Sana Ben Moussa[4] · Joseph Kavitha[5] · Nur Insyirah Mohd Nadzri [6]· Abdullah Yahya Abdullah Alzahrani[4]

[1] Cambrian Consultancy Centre and Industrial Research (CCCIR), Cambridge Institute of Technology, K R Puram, Bengaluru 560036, Karnataka, India

[2] Department of Mechanical Engineering, Cambridge Institute of Technology, K R Puram, Bengaluru 560036, Karnataka, India

[3] Department of Chemistry, Cambridge Institute of Technology, K R Puram, Bengaluru 560036, Karnataka, India

[4] Department of Chemistry, Faculty of Science, King Khalid University, Abha 61413, Saudi Arabia

[5] Department of Basic Sciences, Cambridge Institute of Technology, K R Puram, Bengaluru 560036, Karnataka, India

[6] Center of Excellence Geopolymer & Green Technology (CEGeoGTech), Universiti Malaysia Perlis (UniMAP), Jalan Kangar-Arau 02600, Perlis, Malaysia

---

✉ **S Joseph**

sudhajos.iisc@gmail.com, sudhajoseph.cccir@cambridge.edu.in

✉ **S. Yallappa**

yallappashiralgi5@gmail.com

Abstract

This study investigates the application of machine learning (ML) models to optimize the selective laser melting (SLM) process for AlSi10Mg alloy by establishing processing windows that simultaneously achieve high relative density, low surface roughness, and high hardness. Gaussian Process Regression (GPR), Artificial Neural Network (ANN), and Random Forest (RF) models were trained using experimental data to predict the relationships between laser power, scan speed, and the resulting material properties. The trained models were used to construct processing parameter maps, three-dimensional property surfaces, and contour maps for identifying suitable processing conditions. The results revealed that laser power and scan speed significantly influence all three properties, with scan speed exhibiting a pronounced effect on the predicted responses. For the combined targets of relative density above 99%, surface roughness below 12 μm, and hardness above 120 HV, the predicted processing windows were 225–275 W and 500–1600 mm s^{-1} for GPR, 175–275 W and 800–1600 mm s^{-1} for ANN, and 150–300 W and 900–1600 mm s^{-1} for RF. The experimentally identified processing window was 175–300 W and 700–1500 mm s^{-1}, demonstrating good agreement with the model predictions. The corresponding volumetric energy density ranges were 57–167 J mm^{-3} for GPR, 33–104 J mm^{-3} for ANN, 28–101 J mm^{-3} for RF, and 35–129 J mm^{-3} for the experimental window. The results demonstrate the potential of ML-assisted processing maps for identifying multi-property optimization windows, guiding experimental parameter selection, and reducing reliance on extensive trial-and-error testing.

Keywords Additive manufacturing· AlSi10Mg · machine learning· process optimization· selective laser sintering· property prediction

1. Introduction

Although additive manufacturing provides significant advantages, its extensive use is still limited by the inadequate quality of the manufactured parts. Utilizing advanced machine learning approaches to predict part quality can increase process stability and trustworthiness, thereby facilitating wider industrial integration of additive manufacturing across various industries. Selective laser melting (SLM) of AlSi10Mg offers significant advantages in producing components with better strength than cast components [1-4] and is primarily attributed to the fine microstructure obtained through rapid solidification rates in Additive Manufacturing (AM). However, the ductility of SLMed AlSi10Mg components is often compromised by several factors including residual stresses due to rapid cooling rates, microstructural heterogeneities such as porosity, un-melted particles and bonding defects between layers. And the ductility is a matter of concern for structural applications. The printing of components with required properties is a challenging task. It needs process parameters optimization which depends on costly trial and error process and a huge number of experiments.

The optimization of processing parameters for printing components with indented properties can be done by either experimenting or modelling. Many experimental observations demonstrating the optimization of processing parameters by printing lots of coupons under different processing conditions such as laser power, scan speed and hatch spacing to obtain the interested mechanical properties are available in the literature [5,6]. This kind of work involves huge amount of costly experiments. Several modelling approaches, including analytical models, machine learning (ML) strategies, and empirical models could also be used to do this [7,8]. Empirical models use regression analysis and statistical methods to establish relationship between processing parameters and material properties. ML algorithms are increasingly used nowadays to predict the optimal processing parameters based on a dataset of process conditions and outcomes. In machine learning, methods like neural networks, support vector machines, gaussian process regression and random forests are used to optimise parameters. Physics-based models consider fundamental principles of heat transfer, fluid flow and solidification. It applies Stefan's equation, Rosenthal's equation and Marangoni flow to predict melt pool characteristics. Phase transformation models can be used to predict microstructure evolution and resulting material properties.

Surrogate models were developed by Kamath et al to predict the characteristics of the melt pool with a laser beam speed using limited amount of input data [9]. Better results were obtained by hyper-parameters optimization [9]. Tapia et. al., studied the melt pool depth of single-track 316L stainless steel by Gaussian Process and predicted the melt pool depths for unknown process parameters using responsive surface [10]. The processing windows within which the melt pool shows the required thermal conduction mode in contrast to the keyhole mode were identified in this work. Kappes et al. proposed a Random Forest Network model to optimise the process parameters for SLMed Inconel 718 [12]. The usage of recycled powder and the correlation between pores and keyholes formation to the part orientation and location was shown in this work. Aoyagi et al. constructed the process parameter maps to optimize the processing conditions of CoCr for low porosity using support vector machines [13]. The ML model based on a multivariate Gaussian process developed by Rankouhi et al predicted the properties of a multi-material 316L-Cu for the given processing conditions [14].

Liu et al developed a Gaussian Process Regression model for laser powder bed fusion (LPBF) of AlSi10Mg and reported a larger optimized processing window for printing dense samples with a relative density ≥ 99% [15]. The relative density contour maps to obtain high strength and ductility were identified in this work. Alamri et al [16] used the ML models Artificial Neural Network, Support Vector Regression, Kernel Ridge Regression, Random Forest, Lasso to optimize the process parameters for predicting the properties of the same alloy parts and found optimal window for multi-criteria properties. The selective laser melting of AlSi10Mg-316L was optimized by Miao et al for predicting the density and surface roughness of the printed parts [17]. It was observed that the optimal volumetric energy density (VED) and the composition of the alloy did not show any linear dependency, the laser power and scan velocity influenced the density and the hatch spacing affected the surface roughness. Wang et al established a quantitative relationship between the laser processing parameters and the density of the printed coupons using an ANN model with back propagation algorithm [18]. However, NN generally requires a large training data sets to get an accurate prediction and generating large amount of experimental data will be expensive for the SLM process. A regression tree algorithm was developed by Kamath et al. [11] for optimizing the processing window of 316 SS to obtain high density. A spatial Gaussian process regression model using Bayesian framework was developed to understand the effect of SLM process parameters on the porosity of 17-4 PH stainless steel and the optimized parameters to print the dense parts were identified [19].

Even though there are machine learning approaches correlating the processing parameters and properties of the printed parts on SLMed AlSi10Mg available in the literature, the process parameter maps for the optimum combination of properties reported are very few. In this work, the machine learning models Gaussian Process Regression (GPR), Artificial Neural Network (ANN) and Random Forest (RF) will be developed to generate the processing parameter maps for the optimization of combination of properties of SLMed AlSi10Mg. There are studies on ML models whereas GPR and RF models have not been studied much. The processing parameter maps were not reported in many of the work. The properties such as relative density, surface roughness and hardness will be studied in this work as the relative density and surface roughness are the major concerns that decides the mechanical properties of the additive manufactured components in addition to the microstructure. Then the optimal region for printing components with the merged criteria of relative density > 99%, surface roughness < 12 μm, and hardness > 120 HV will be predicted from the contour maps generated by ML models. The volumetric energy density for these optimal regions will also be predicted. In addition, our study predicts the uncertainty maps using Gaussian Process Regression (GPR) to quantify the confidence associated with predicted AlSi10Mg properties across the LPBF processing space beyond conventional property-prediction maps. This uncertainty-aware framework enables identification of statistically robust processing windows, distinguishing reliable optima from regions where predictions remain data-limited. Further, the findings of this research work would contribute to the development of guidelines for optimizing laser melting processes of AlSi10Mg to obtain the properties in the as-printed condition. It is important as thin walled components and complex parts sometimes cracks and distorts respectively while heat treatment.

2. Materials and Methods

2.1 Methodology

The correlation between the laser melting process parameters and the properties of the printed coupons will be established using ML models, GPR, ANN, and RF. In the present study, these ML models are employed to predict the relative density (ρ), surface roughness (Ra) and hardness (HV) based on four key process parameters laser power, scan speed, hatch distance and layer thickness. The experimental data collected from the literature was used to train the ML models.

2.1 Data collection

The data for the selective laser melted AlSi10Mg alloy was collected from the literature [16] and used for training all the ML models studied. The laser melting process parameters such as laser power, laser scanning speed, hatch spacing, and layer thickness and the characteristics of the printed coupons such as relative density, surface roughness and hardness were collected. The experimental data set of 221 data for density, 55 data for hardness and 114 data for surface roughness has been used to generate these maps. The potential biases such as machine settings, powder characteristics and measurement methods has been carefully checked to avoid inconsistencies. 80% of data was used for training and 20% for validation. The data collected was first pre-processed before giving as an input to the ML models and it involves: (i) Normalization of the processing parameters in order to make them non-dimensional and (ii) standardization of the target variables to the zero mean and a standard deviation of 1. The tuning parameters of the models were optimized to get reasonably good accuracy and minimum error. The trained models were used to predict the surface maps and contour maps.

2.2 Gaussian process regression (GPR)

GPR is a probabilistic model used to predict the properties of the printed coupons and its uncertainty. It can be described by a mean function (m) and the covariance function (k) in GPR as [21].

$$\text{Property}\ (P, v, h, t) = GP\ [m(P, v, h, t), k(P, v, \mathrm{h}, \mathrm{t}, P', v', \mathrm{h}', \mathrm{t}')] \quad \ldots\ldots\ldots\ldots\ldots\ldots (1)$$

where P is the laser power, v is the scan speed, h is the hatch spacing and t is the layer thickness. The Property could be the relative density or surface roughness or hardness of the printed coupon. P, v, h, t are the training data points and P', v', h', t' are the predicting points. The

hyperparameters were obtained by training the model using the input data. Then the output 'Property' corresponding to a new processing parameter set (P', v', h$'$, t$'$) was predicted as a Gaussian distribution. The kernels squared exponential (SE) and white were used as the covariance function.

The general framework of GPR approach is shown in Figure 1. The processing parameters (P, v, h and t) and the properties (relative density, surface roughness and hardness) were used as input and output, respectively. The experimental data collected from the literature was used to train and test the model. The trained ML algorithm were used to generate the response surface on the input data. Then the contour maps were obtained from the response surface to predict the required properties. The GPR model was studied as it gives good results using less amount of training data sets.

Following earlier work on ML-assisted property prediction in LPBF AlSi10Mg [20], the present study extends the methodology by employing multiple surrogate models (GPR, ANN, and RF) to simultaneously predict several material properties rather than focusing on a single one.

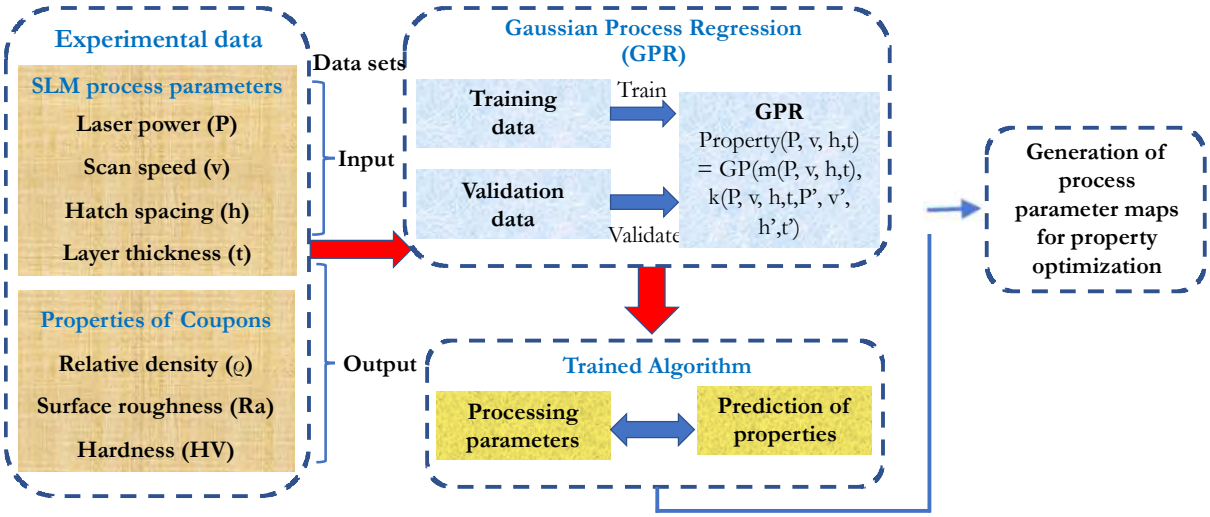


Figure 1 A general framework of GPR modelling approach

2.3 Artificial Neural Networks (ANN)

ANNs are powerful tools used to model complex, nonlinear and relationships between the input and output data [22]. The Multi-Layer Perceptron (MLP) is the most commonly used among different types of ANNs as it can handle noisy data and ignore irrelevant inputs while learning patterns. An MLP has number of layers including input layer, one or more hidden layers and an output layer, Figure 2. There are 4 neurons in the input layer, one neuron in the output layer and 3 hidden layers with 512, 256 and 128 neurons. This architecture has been optimized and the overfitting has been controlled. The input parameter (x_i) to the model are laser power, scan speed, hatch distance and layer thickness and the output parameter (y_k) is either relative density or surface roughness or hardness. The neurons in one layer are fully connected to the neurons in the other layers. The output of the neurons is calculated by applying an activation function to a weighted sum of its inputs. The RELU function is used as an activation function for all layers.

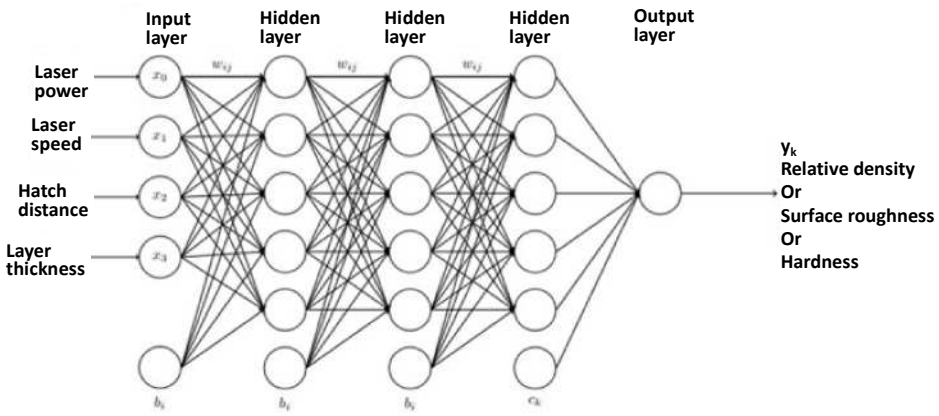


Figure 2 Schematic of an ANN model with input parameters (x_i), output parameters (y_k), weights (w_{ij}) and bias (b_i)

2.4 Random Forest (RF)

RF is an ensemble ML technique which trains the multiple decision trees and select the ensemble output with the best overall performance. This technique was applied by Alamri et al. [16] to predict individual properties of SLMed AlSi10Mg, alongside ANN and SVR were also used to define a common optimal region for all desired material properties. It is well-suited for regression tasks involving complex and nonlinear relationships such as predicting relative density, surface roughness and hardness in additive manufacturing processes. The model

constructs an ensemble of *N* decision trees, denoted as: $\{R_1(X), R_2(X), ..., R_n(X)\}$, where $X = \{x_1, x_2, ..., x_p\}$ is a *p*-dimensional input vector representing the selected process parameters. Each decision tree in the forest is trained on a bootstrapped sample of the training data, and feature selection at each node is randomized. This intentional randomness ensures that individual trees are de-correlated, which reduces the model's variance and enhances its generalization ability. For each test sample, the final prediction of the RF model is computed as the mean of the predictions from all individual trees:

$$\hat{Y} = (1/N) \times \sum R_n(X), \text{ where } n = 1 \text{ to } N \quad \text{..... (2)}$$

RF improves the predictive accuracy by taking the average to control overfitting [7].

3. Results and discussion

The machine learning models GPR, ANN and RF have been trained using the experimental data and trained models were used to generate the surface and contour maps of relative density, surface roughness and hardness of the selective laser melted AlSi10Mg alloy. The results are presented as a function of laser power and scan speed as these parameters are observed to mainly affect the properties. The fixed values of hatch spacing 82 µm and layer thickness 60 µm have been used for all the modelling.

3.1 Model predictions on relative density

Table 1 shows the optimized tuning parameters and the accuracy of the different ML models for predicting the relative density of selective laser melted AlSi10Mg alloy. The goodness of fit of the model R^2 score, Root Mean Squared Error (RMSE) and Mean Absolute Error (MAE) of the predictions are mentioned in the table.

Table 1. Optimal tuning parameters and accuracy of the ML models for predicting relative density of selective laser melted AlSi10Mg

Model	Parameters	Accuracy		
		R^2	RMSE	MAE
GPR	$\ell = 0.325$, $\sigma^2 = 0.759$	0.757	0.5738	0.2863
ANN	η=0.0005, λ=0.0005, p=0.1	0.885	0.3914	0.2256
RF	n-estimators = 100	0.909	1.6180	0.8940

Note: GPR = Gaussian Process Regression, ANN = Artificial Neural Network, RF = Random Forest, R^2 = coefficient of determination, MSE = mean squared error, MAE = mean absolute error, ℓ = length-scale, σ^2 = signal variance, η = learning rate, λ = regularization parameter, p = dropout probability.

The predicted density versus actual density obtained from the GPR, ANN and RF models after training and validation of the models is shown in Figure 3. The perfect prediction is shown by the dotted line where the prediction matches with the experimental values used for training the model. For all the three models, the perfect prediction was observed on the higher density regions as the points lie on the line. The scattered points were observed in the lower density regions and the error of the prediction will be more if the point is far away from the line. The R^2 value in Table 1 implies good accuracy for all the models and the highest accuracy is shown by the random forest model. The highest R^2 score of 0.909 and RMSE of 1.618 with 100 estimators is attained by the random forest, followed by ANN and GPR models. The R^2 value of 0.885 and RMSE of 0.0.3914 was achieved by ANN with tuning parameters η=0.0005, λ=0.0005, p=0.1 and the GPR model showed the R^2 value of 0.757 and RMSE of 0.5738 with tuning parameters ℓ = 0.325, σ^2 = 0.759.

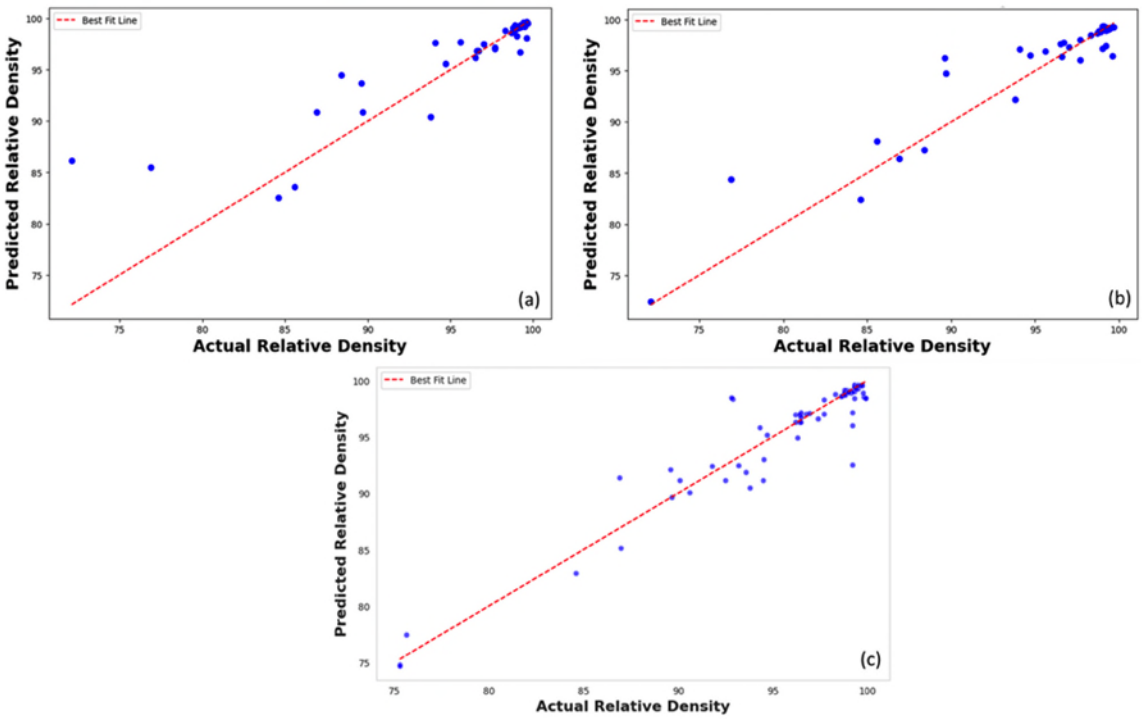


Figure 3 Accuracy of the models for relative density (%) prediction of selective laser melted AlSi10Mg (a) GPR (b) ANN and (c) RF

The process parameter maps predicted by GPR, ANN and RF models for relative density of SLMed AlSi10Mg are shown in Figure 4 (a, c and e) and the corresponding contour maps are shown in Figure 4 (b, d and f). The input for the predictions contained laser power from 100 W to 950 W, scan speed from 200 mm s^{-1} to 3000 mm s^{-1} hatch spacing 0.05 mm to

0.25 mm and the layer thickness from 0.02 to 0.04mm. The experimental data set of 221 data has been used to generate these maps and it is possible to extract 1000 of datasets from these ML models generated maps. Thus, these maps can be used to predict the property for the unknown process parameters. The laser processing parameters and the corresponding properties extracted from these maps were found to fall within the experimental range as well as outside the range. The blue colour is the lower density region and the red colour is the higher density region. In general, all models showed a strong effect of laser power and scan speed on the density of the printed coupons. Similar results were observed by the ANN model by Alamri et al [16]. The models ANN and RF showed strong sensitivity to scan speed. The GPR model predicted low density in the low power and high velocity regime. This matches with the experimental observations as the low volumetric energy density at this regime insufficient to form stable and large molten pools.

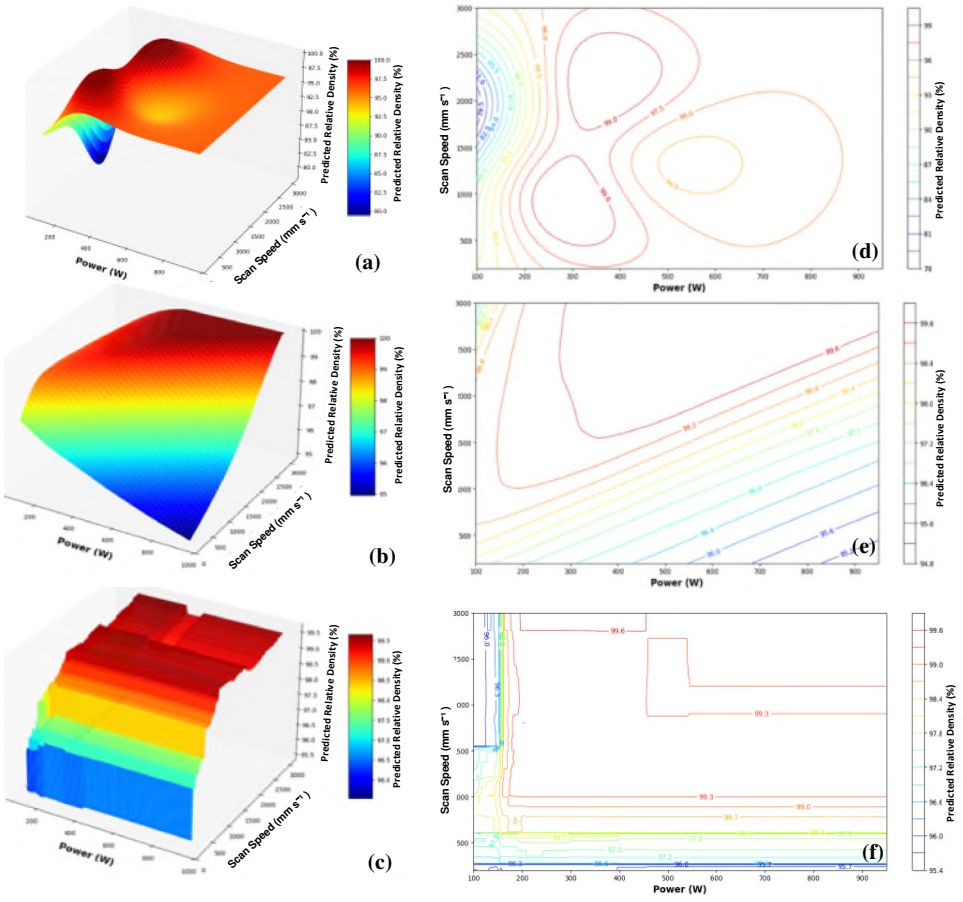


Figure 4 Relative density predictions of selective laser melted AlSi10Mg by ML models (a, b and c) Processing parameter maps predicted by GPR, ANN and RF and (d, e and f) Contour maps predicted by GPR, ANN and RF

The optimized processing conditions for printing AlSi10Mg having relative density > 99% was estimated from the predicted maps. According to GPR model two regions were observed showing relative density > 99%: low laser power with low scan speed and low laser power with high scan speed. These regions fall in the laser power 200-400W and scan speed 500-1250 mm $s^{-1}$and laser power 250-450W and scan speed 1750-2750 mm s^{-1}ranges. This range matches with the work reported by Liu et al [20] and their predictions showed a maximum laser power of 400W and a scan speed of 500-2500 mm s^{-1}. The low laser power and high scan speed combination results in inadequate energy input and cause defects such as keyholes, balling or bead-up which may affect the density of the specimen [9,15,23]. Hence a laser power 200-400W and scan speed 500-1250 mm s^{-1}combination was considered suitable for printing high density AlSi10Mg parts. A relatively wide processing window was predicted by the ANN model in the range with laser power 150-900W and scan speed 1000-3000 mm s^{-1}. The RF model also predicted a wide region similar to the ANN model. These results demonstrate that lot of printing options are available to achieve high density in SLMed AlSi10Mg components. All the three models predicted a laser power of 200-400W and a scan speed of 500-1250 mm s^{-1} ranges for printing components with higher relative density > 99%. This matches with the experimental findings as well as other model predictions [15]. The observed trends in relative density follow the fundamental physics. The resulting volumetric energy density at low laser power and/or high scan speed is insufficient to fully melt the powder particles producing shallow and discontinuous melt pools that cause lack-of-fusion porosity [24]. In contrast, the excessive energy input at very high laser power or low scan speed promotes deep keyhole formation and unstable melt pool dynamics, increasing the likelihood of gas entrapment and defect generation. Stable and continuous melt pools occur within the intermediate VED range predicted by all three models, promoting complete powder consolidation and minimizes porosity [25].

Lower densities below 95% was predicted in the low power regime < 200W by the GPR model, high power around 1000W and low scan speed below 500 mm $s^{-1}$by the ANN model and a low scan speed of 500 mm s^{-1} by the RF model. This matches with the experimental observations as these processing conditions either lead to insufficient or excessive energy input.

3.2 Model predictions on surface roughness

The optimized tuning parameters and the accuracy of the different ML models for predicting the surface roughness of selective laser melted AlSi10Mg is shown in Table 2. The R^2 score, RMSE

and MAE values of the predictions are mentioned in the table. The predicted and the actual surface roughness obtained from GPR, ANN and RF models are shown in Figure 5. The scattered points were observed for all the models and it was less scattered for random forest. The accuracy of the models is reasonably good and the random forest showed the highest accuracy among all the models, Table 2. The highest R^2 score of 0.902 and RMSE of 1.618 µm with 200 estimators is attained by the random forest, followed by ANN and GPR models. The R^2 value of 0.811 and RMSE of 0.3873 µm was achieved by ANN with tuning parameters η=0.0005, λ=0.0005, p=0.1 and the GPR model showed the R^2 value of 0.622 and RMSE of 0.5612 µm with tuning parameters $\ell = 0.325$, $\sigma^2 = 0.759$.

Table 2. Optimal tuning parameters and accuracy of the ML models for predicting the surface roughness of selective laser melted AlSi10Mg

Model	Parameters	Accuracy		
		R^2	RMSE (µm)	MAE(µm)
GPR	$\ell = 0.325$, $\sigma^2 = 0.759$	0.622	0.5612	0.471
ANN	η=0.0005, λ=0.0005, p=0.1	0.811	0.3873	0.291
RF	n-estimators = 200	0.902	1.6180	3.2859

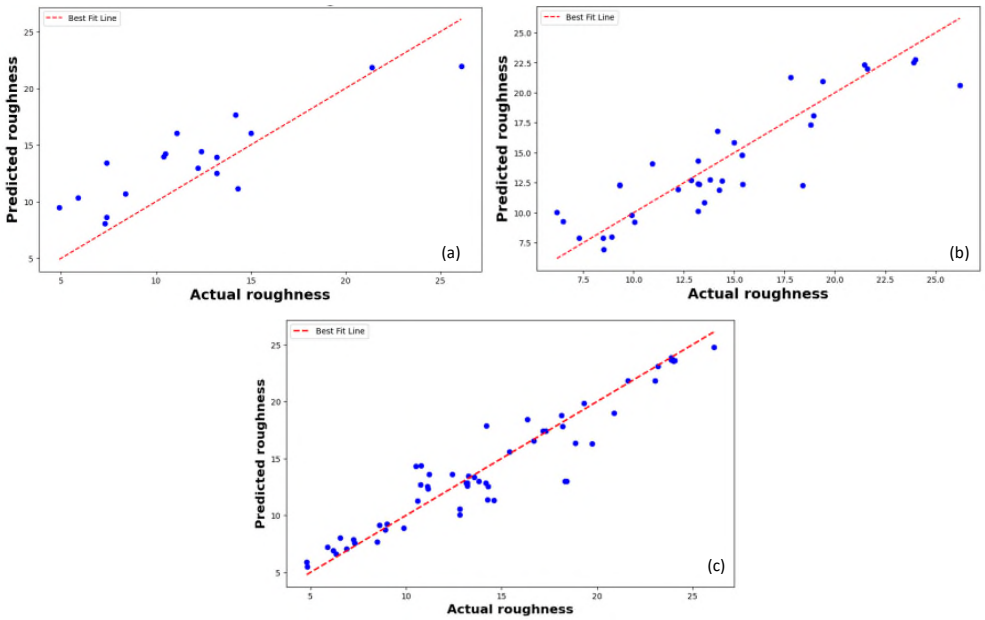


Figure 5 Accuracy of the models for surface roughness (µm) prediction of selective laser melted AlSi10Mg (a) GPR (b) ANN and (c) RF

The process parameter maps for surface roughness of SLMed AlSi10Mg predicted by GPR, ANN and RF models are shown in Figure 6 (a, c and e) and the respective contour maps are shown in Figure 6 (b, d and f). The input for this prediction contained laser power from 109 W to 274 W, scan speed from 200 mm s^{-1} to 3000 mm s^{-1} hatch spacing from 0.04 mm to 0.105 mm and layer thickness from 0.02 to 0.03. The lower surface roughness values are represented by blue colour and the red colour represents higher surface roughness values. In general, all the models showed strong impact of scan speed on the surface roughness. The optimized window for printing AlSi10Mg parts with surface roughness < 12 μm was found to be: GPR model predicted a regime of laser power 160-260W and scan speed 200-1500 mm s^{-1}, ANN model predicted a regime of laser power 180-260W and scan speed 500-2000 mm s^{-1} and RF model predicted regimes of laser power 125-300W and 200-300W and scan speed 300-900 mm s^{-1} and 500-2200 mm s^{-1}. RF model predicted a wide range of scan speed for fabricating specimens with surface roughness <12 μm. Good surface finish cannot be achieved at extremely low or high scan speed. The balling can occur along the laser scan paths at higher scan speed due to the molten pool elongation and its subsequent rupture under Rayleigh instability to reduce surface tension [26,27]. The surface roughness of SLM parts is mainly affected by balling. The surface roughness also increase under low laser power and/or high scan speed combination as the energy input is insufficient to fully melt the powder bed, leading to discontinuous tracks and partially fused particles adhering to the surface [17]. At the opposite extreme, excessive energy from high power or low scan speed can destabilise the melt pool, causing spatter ejection and balling which breakup the melt track into beads under surface tension which solidify as irregular surface irregularities. Further, the low volumetric energy density values would cause incomplete melting of the powder on the surface leading to high surface roughness. It was observed that a regime with laser power 180-260W and scan speed 500-1500 mm s^{-1} was predicted by all the ML models for fabricating specimens with surface roughness < 12 μm.

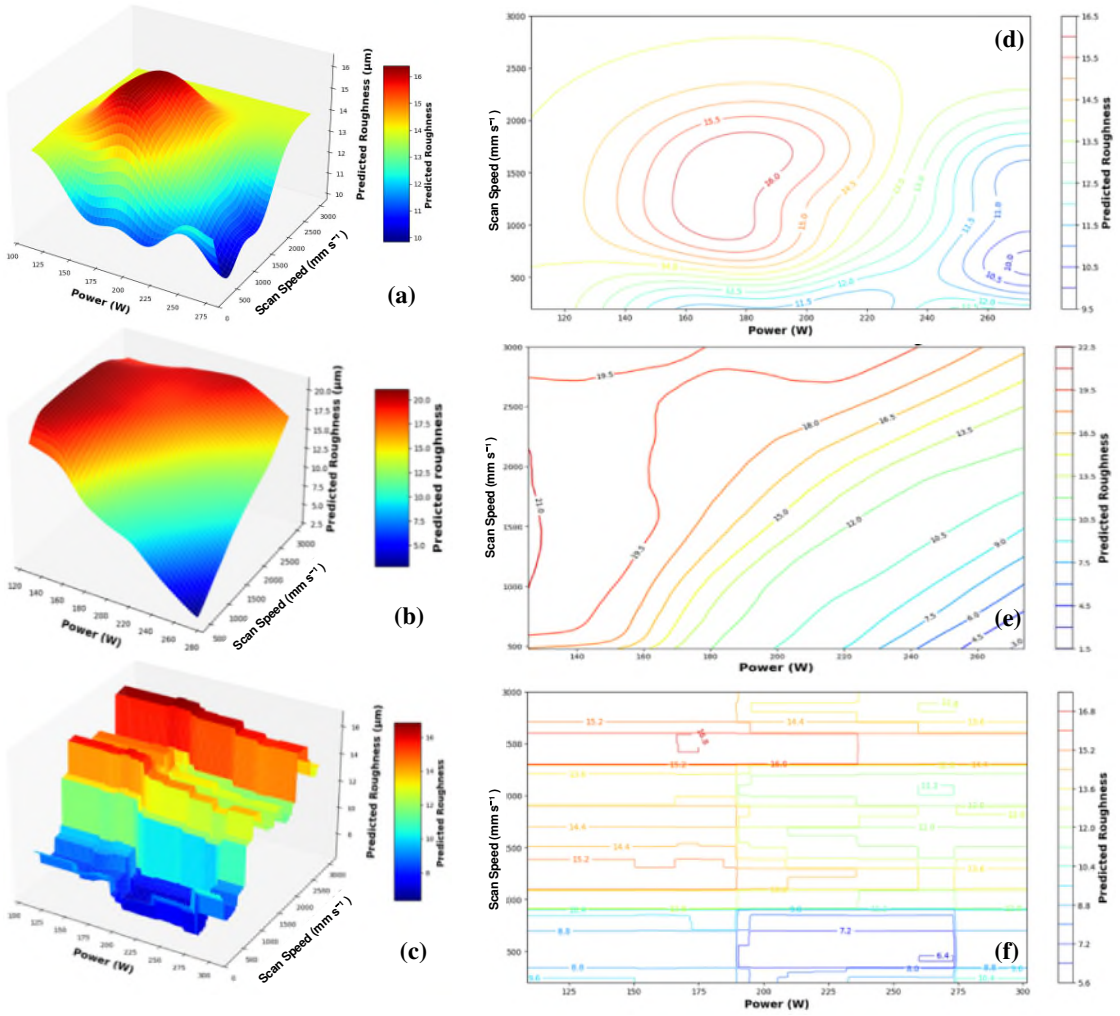


Figure 6 Roughness predictions of selective laser melted AlSi10Mg by ML models (a, b and c) Processing parameter maps predicted by GPR, ANN and RF and (d, e and f) Contour maps predicted by GPR, ANN and RF

3.3 Model predictions on hardness

The optimized tuning parameters and the accuracy of the different ML models used for predicting the hardness of selective laser melted AlSi10Mg is shown in Table 3. The R^2 score, RMSE and MAE of the predictions are mentioned.

Table 3. Optimal tuning parameters and accuracy of the ML models for predicting the hardness of selective laser melted AlSi10Mg

Model	Parameters	Accuracy		
		R^2	RMSE (HV)	MAE (HV)
GPR	$\ell = 0.325$, $\sigma^2 = 0.759$	0.778	0.6512	0.537
ANN	η=0.0005, λ=0.0005, p=0.1	0.945	0.5612	0.143
RF	n-estimators = 200	0.927	1.814	1.713

Figure 7 shows the plot of predicted hardness versus actual hardness obtained from GPR, ANN and RF models. The models showed reasonable accuracy and the ANN showed the highest accuracy among all the models, Table 3. Alamri et al [16] has also reported ANN showed more predictability than SVR, KRR, RF and lasso progression. The ANN achieved a highest R^2 of 0.945 and RMSE of 0.5612 HV with tuning parameters η=0.0005, λ=0.0005, p=0.1, followed by RF and GPR models. The RF model resulted in an R^2 of 0.927 and RMSE of 1.814 HV with 200 estimators and the GPR model showed in an R^2 of 0.778 and RMSE of 0.6512 HV with tuning parameters $\ell = 0.325$, $\sigma^2 = 0.759$.

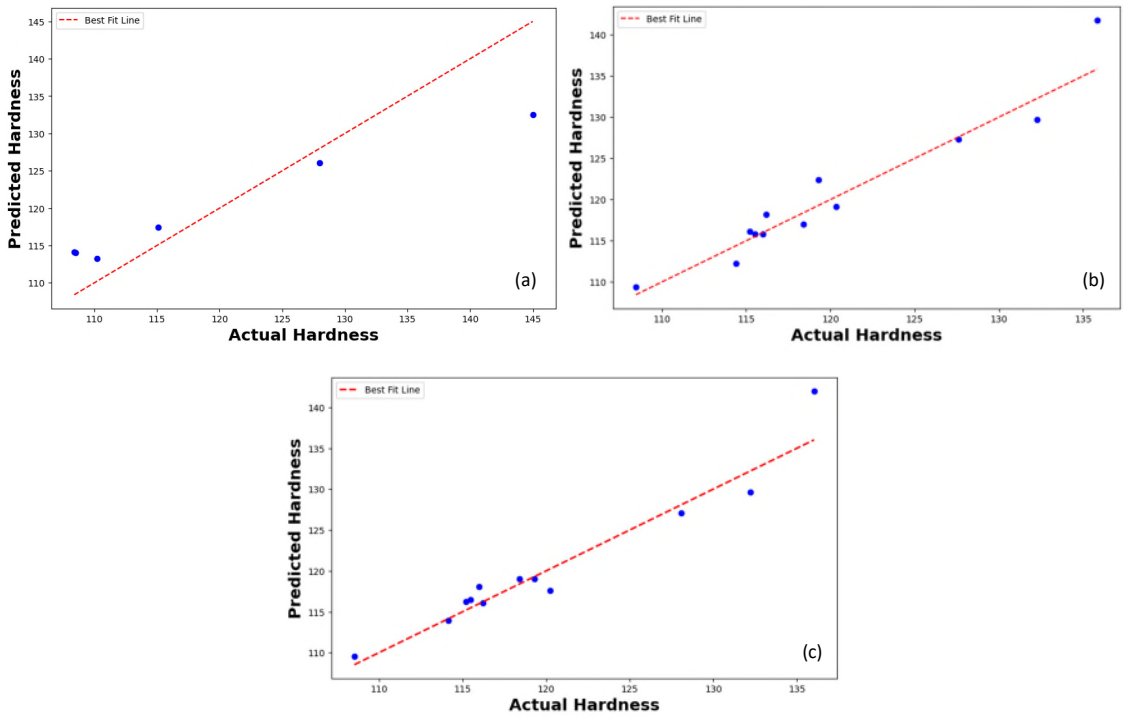


Figure 7 Accuracy of the models for hardness (HV) prediction of selective laser melted AlSi10Mg (a) GPR (b) ANN and (c) RF

Figure 8 (a, c and e) shows the process parameter maps for hardness of SLMed AlSi10Mg predicted by GPR, ANN and RF models and the respective contour maps are shown in Figure 8 (b, d and f). The input for this prediction contained laser power from 109 W to 400 W, scan speed from 200 mm s^{-1} to 1600 mm s^{-1} hatch spacing from 0.05 mm to 0.25 mm and layer thickness 0.02 to 0.05 mm. In general, all the models showed the influence of laser power and scan speed on the hardness values and the scan speed has a stronger effect than the power.

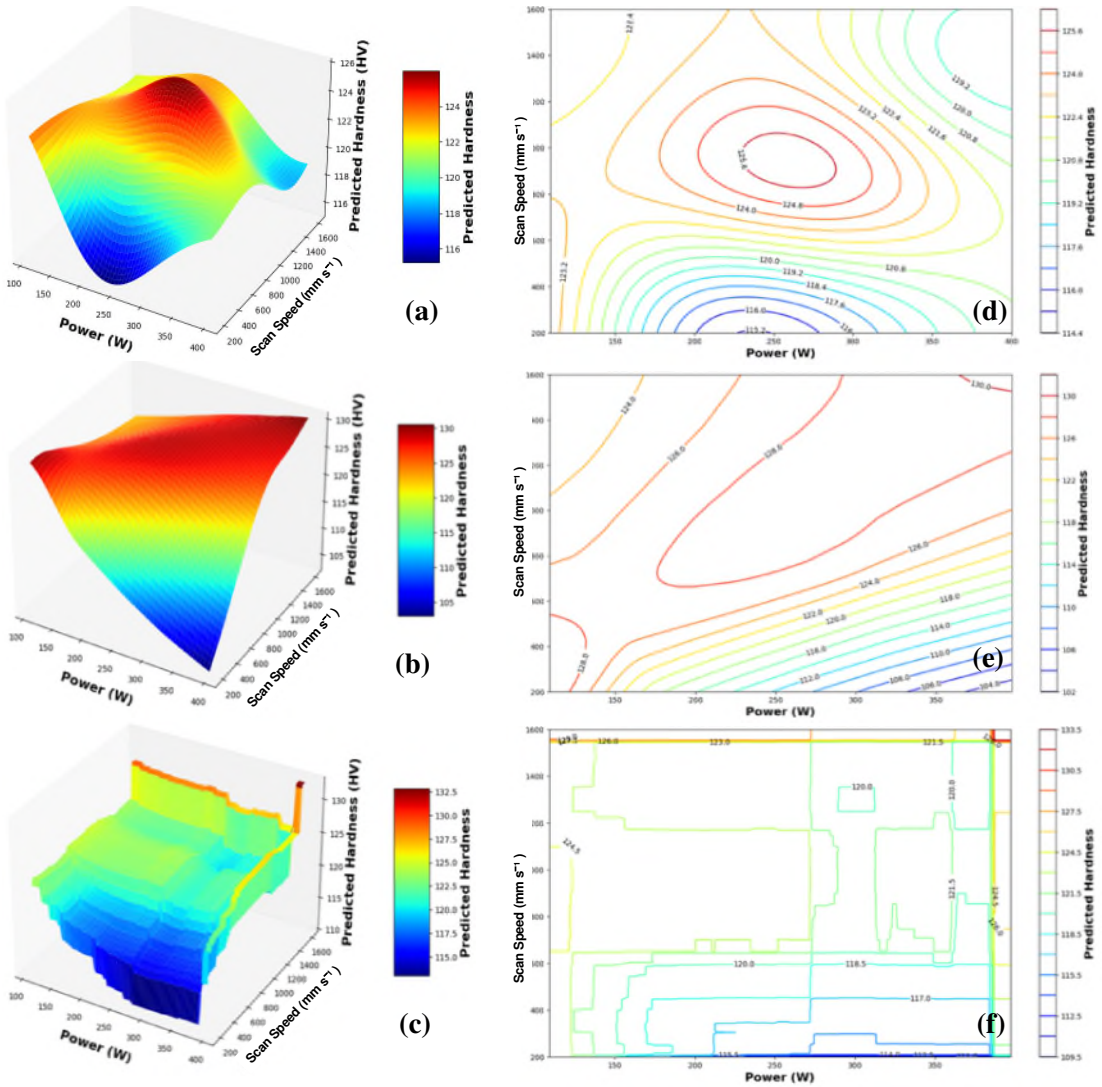


Figure 8 Hardness predictions of selective laser melted AlSi10Mg by ML models (a, b and c) Processing parameter maps predicted by GPR, ANN and RF and (d, e and f) Contour maps predicted by GPR, ANN and RF

Lower scan speed can cause higher energy input per unit length which helps in better fusion but can overheat the material. In addition, it causes coarse microstructure which lowers

the hardness values. Higher scan speed leads to faster cooling resulting in refined grains in aluminium alloys which usually increases the hardness. The hardness trends predicted by the ML models can be explained by the experimental observations made by et al [28,29]. High hardness in this alloy is linked to rapid solidification, which produces a fine aluminium (α-Al) matrix reinforced by silicon both dissolved in the metal and as nano sized particles at the cell boundaries [28]. These results are consistent with the experimental findings that SLM-processed AlSi10Mg exhibits a fine cellular microstructure with uniformly distributed Si, which enhances hardness and mechanical strength [29]. At low volumetric energy density (VED), incomplete melting leaves porosity and uneven, coarse regions that lower hardness. At very high energy input, slower cooling allows the microstructure to coarsen, reducing this strengthening effect. Similar observations were made by Lv et al., who demonstrated that both LPBF parameters and subsequent heat treatments can significantly alter the microstructure and mechanical properties of AlSi10Mg [30]. The optimized processing window for fabricating AlSi10Mg parts by SLM with a hardness value > 120 HV was found to be: GPR model predicted a regime of laser power 100-400W and scan speed 200-1600 mm s^{-1}, ANN model predicted a regime of laser power 150-400W and scan speed 200-1600 mm s^{-1} and RF model predicted a regime of laser power 100-400W and scan speed 600-1600 mm s^{-1}. All the models predicted a regime with the laser power 150-400W and scan speed 600-1600 mm s^{-1} for fabricating specimen with hardness > 120 HV. The overall consistency of the ML model predictions with experimental studies validates their suitability as surrogate tools for process optimization. This agrees with the multi-objective optimization work by Toprak and Doğdu, who showed that optimal parameter balancing is necessary to simultaneously achieve high hardness, density, and surface quality in LPBF AlSi10Mg [31].

3.4 Optimized processing parameter maps

The predicted process parameter maps for optimal combination of properties for selective laser melting of AlSi10Mg by GPR, ANN and RF models are shown in Figure 9 (a, b, c). The optimized maps for the experimental data is also shown for comparison, Figure 9(d). A criteria with relative density > 99%, surface roughness < 12 μm and hardness > 120 HV was defined to obtain the optimized processing window. The respective individual optimized regions have been merged and the common region that overlaps all three criteria is highlighted in red border in the Figure.

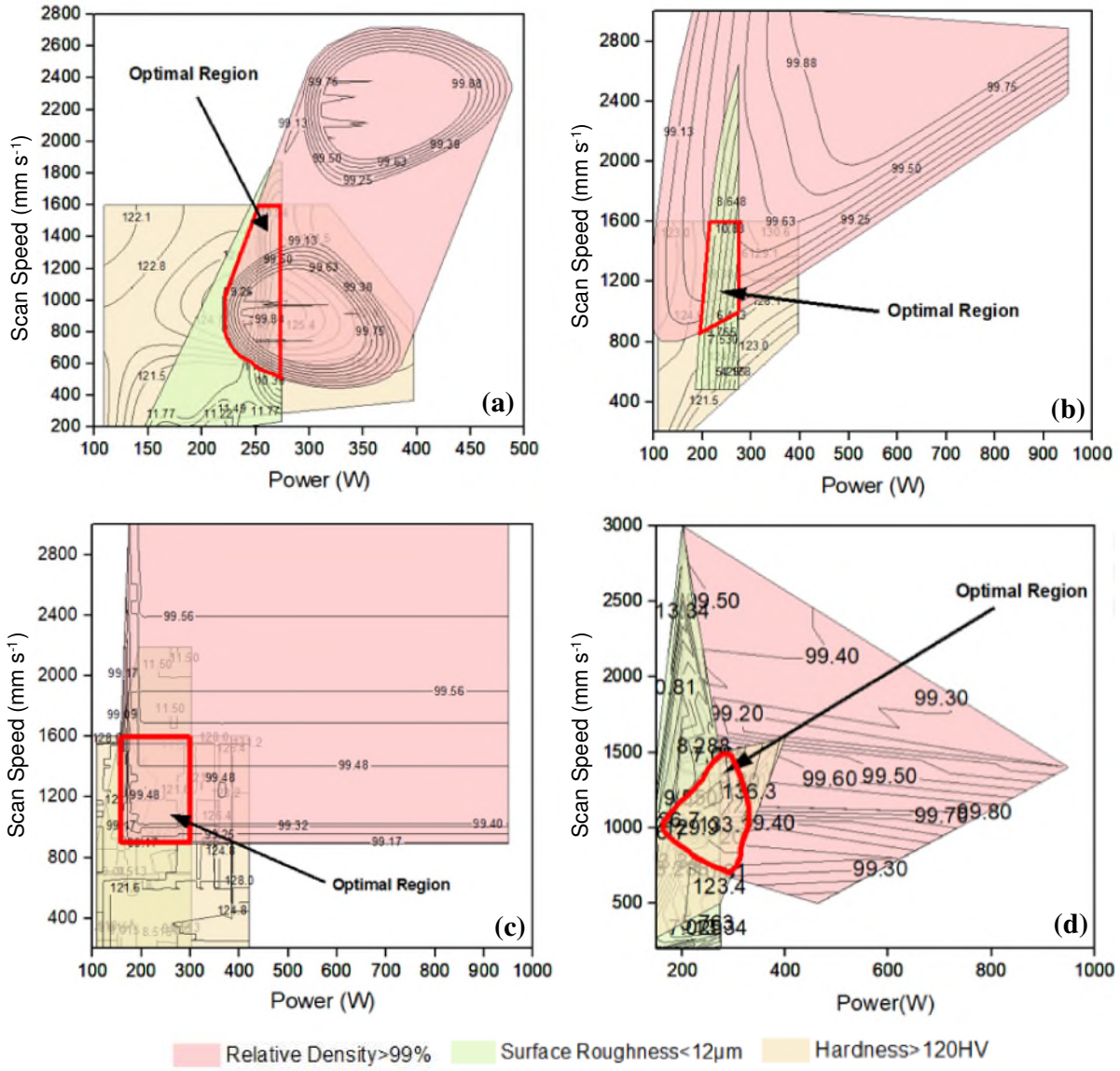


Figure 9 The optimal region for selective laser melted AlSi10Mg parts with the merged criteria of relative density > 99%, surface roughness < 12 μm, and hardness > 120 HV predicted by the ML models (a) GPR (b) ANN (c) RF and (d) Experimental results for comparison

The region having laser power 225 - 275 W and scan speed 400 - 1600 mm s^{-1} was found to provide optimal combination of relative density, surface roughness and hardness for SLMed AlSi10Mg according to GPR. ANN and RF predicted the optimal region in the window having laser power 175-275 W and scan speed 800-1600 mm s^{-1} and laser power 150-300 W and scan speed 900-1600 mm s^{-1} respectively. The optimal region reported was narrow in the range 250-300W and 1000-1250 mm s^{-1} [15]. The experimental data showed the optimal region in the range of 175-300 W laser power and 700-1500 mm s^{-1} scan speed and our results fall

well in the experimental range. The high quality AlSi10Mg components can be produced by printing in the above mentioned optimal regions which ensures better mechanical properties and performance.

The volumetric energy density (VED) was calculated for the optimal region for both the experiment data and machine learning models' predictions as this value gives better understanding than the individual processing parameters. The volumetric energy density is:

$$E = \frac{P}{vht} \quad \text{..... (3)}$$

Where P - laser power, v - scan speed, h - hatch spacing and t - layer thickness.

The volumetric energy density for the optimal region was found to be in the range: GPR- 57 to 167 J mm^{-3}, ANN- 33 to 104 J mm^{-3}, RF- 28 to 101 J mm^{-3} and experiment – 35 to 129 J mm^{-3}. Both the laser processing parameter window and the volumetric energy density range for the optimal combination of properties predicted by ML models show good agreement with the experimental predictions. Hence these processing parameter maps generated in this work can be used for predicting the laser parameters for the defined property values. The GPR model predicted the VED range a little higher than the experimental observation. Thus this model gives some more choices of printing parameters other than the experimentally studied values for property optimization.

3.5 Uncertainty maps

The uncertainty maps of GPR model for the prediction of relative density, surface roughness and hardness is shown in Fig. 10. The GPR model exhibited low prediction errors across the investigated process-parameter space, confirming its capability to accurately predict the density, surface roughness, and hardness of SLMed AlSi10Mg. The maximum prediction error is about only 1.35% for relative density and about 1.1% for both surface roughness and hardness, and it falls below 0.5 % over most of the parameter space (Figure 10a–c). Density has the widest error range (up to ~1.4 %) because it is most sensitive to the transition between lack-of-fusion porosity and fully dense melting, whereas roughness and hardness vary more smoothly and give smaller, flatter error surfaces. The localized peaks are associated with specific combinations of laser power and scan speed, indicating increased prediction uncertainty in these process regimes. Overall, the consistently low error surfaces demonstrate

the robustness of the GPR model for process–property prediction and its potential for subsequent parameter optimization of SLMed AlSi10Mg. These error maps provide an additional measure of confidence for selecting suitable processing regions.

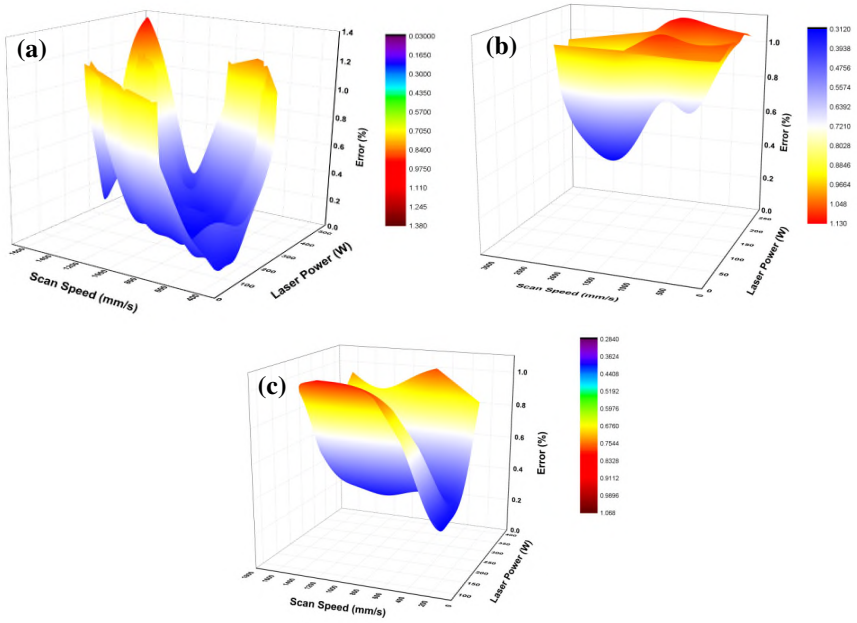


Fig. 10 Error maps showing the uncertainty in the prediction of (a) relative density, (b) surface roughness and (c) hardness by the GPR model

4. Conclusion

This study generated machine learning-assisted processing maps for optimizing selective laser melting of AlSi10Mg, enabling the identification of suitable laser power and scan speed combinations for achieving targeted combination of material properties.

- The GPR, ANN, and RF models successfully captured the relationships between laser power, scan speed, and the relative density, surface roughness, and hardness of AlSi10Mg.
- A significant effect of laser power and scan speed on the relative density of the printed parts was observed. The ANN and RF models showed strong sensitivity to scan speed.

All the models predicted a regime having laser power 200-400W and scan speed 500-1250 mm s^{-1} for printing AlSi10Mg with relative density above 99%.

- The models identified promising processing regimes for achieving relative density above 99%, surface roughness below 12 μm, and hardness above 120 HV, demonstrating their potential for multi-property process optimization. The optimal processing windows predicted by GPR (225–275 W, 500–1600 mm s^{-1}), ANN (175–275 W, 800–1600 mm s^{-1}), and RF (150–300 W, 900–1600 mm s^{-1}) showed good agreement with the experimentally identified window (175–300 W, 700–1500 mm s^{-1}).
- The corresponding volumetric energy density ranges were 57–167 J mm^{-3} for GPR, 33–104 J mm^{-3} for ANN, 28–101 J mm^{-3} for RF, and 35–129 J mm^{-3} for the experimental window. The ML models also identified candidate processing conditions beyond the experimentally investigated regime, offering opportunities to explore additional parameter combinations.
- The error maps of GPR provided an additional measure of model reliability and can be used with the predicted mechanical property surfaces to identify processing regions where both the desired mechanical response and prediction confidence are required.

Declarations Competing Interests The authors have no relevant financial or non-financial interests to disclose.

Data availability statement: Data will be made available on request.

References

[1] Bai, Y., Yang, Y., Xiao, Z., Zhang, M. and Wang, D. (2018), "Process optimization and mechanical property evolution of AlSiMg0. 75 by selective laser melting", Materials & Design, Elsevier, Vol. 140, pp. 257–266, doi: 10.1016/j.matdes.2017.11.045.

[2] Kempen, K., Thijs, L., Van Humbeeck, J. and Kruth, J.-P. (2015), "Processing AlSi10Mg by selective laser melting: parameter optimisation and material characterisation", Materials Science and Technology, SAGE Publications Sage UK: London, England, Vol. 31 No. 8, pp. 917–923, doi: 10.1179/1743284714Y.00000007

[3] Read, N., Wang, W., Essa, K. and Attallah, M.M. (2015), "Selective laser melting of AlSi10Mg alloy: Process optimisation and mechanical properties development", Materials & Design (1980-2015), Elsevier, Vol. 65, pp. 417–424, doi: 10.1016/j.matdes.2014.09.044

[4] Yan, Q., Song, B. and Shi, Y. (2020), "Comparative study of performance comparison of AlSi10Mg alloy prepared by selective laser melting and casting", Journal of Materials Science & Technology, Elsevier, Vol. 41, pp. 199–208, doi: 10.1016/j.jmst.2019.08.049

[5] Aboulkhair, N.T., Everitt, N.M., Ashcroft, I. and Tuck, C. (2014), "Reducing porosity in AlSi10Mg parts processed by selective laser melting", Additive Manufacturing, Vol. 1, pp. 77–86, doi: 10.1016/j.addma.2014.08.001.

[6] Krishnan, M., Atzeni, E., Canali, R., Calignano, F., Manfredi, D., Ambrosio, E.P., Iuliano, L., et al. (2014), "On the effect of process parameters on properties of AlSi10Mg parts produced by DMLS", Rapid Prototyping Journal, Elsevier, Vol. 20 No. 6, pp. 77–86, doi: 10.1108/RPJ-03-2013-0028

[7] DebRoy, T., Mukherjee, T., Wei, H.L., Elmer, J.W. and Milewski, J.O. (2021), "Metallurgy, mechanistic models and machine learning in metal printing", Nature Reviews Materials, Nature Publishing Group UK London, Vol. 6 No. 1, pp. 48–68, doi: 10.1038/s41578-020-00236-1

[8] Miao, B., Lin, G.-Q., Zhang, Y., Cheng, Y.-W. and Yang, H. (2026), "Machine learning applications in metallic materials: Recent advances and future perspectives", Journal of Alloys and Compounds, Elsevier, p. 187486. Doi: doi.org/10.1016/j.jallcom.2026.187486.

[9] Kamath, C. and Fan, Y.J. (2018), "Regression with small data sets: a case study using code

surrogates in additive manufacturing", Knowledge and Information Systems, Vol. 57, pp. 475–493, doi: 10.1007/s10115-018-1174-1

[10] Tapia, G., Khairallah, S., Matthews, M., King, W.E. and Elwany, A. (2018), "Gaussian process-based surrogate modeling framework for process planning in laser powder-bed fusion additive manufacturing of 316L stainless steel", The International Journal of Advanced Manufacturing Technology, Springer, Vol. 94, pp. 3591–3603, doi: 10.1007/s00170-017-1045-z

[11] Zhang, Z., Liu, Z., Li, Y., Sun, F., Wu, C. and Dong, S. (2026),
[38] "Machine learning-assisted screening of transition metal-doped nickel phosphide electrocatalysts for hydrogen evolution reaction", Journal of Alloys and Compounds, Elsevier, p. 187427, doi: 10.1016/j.jallcom.2026.187427

[12] Kappes, B., Moorthy, S., Drake, D., Geerlings, H. and Stebner, A. (2018), "Machine learning to optimize additive manufacturing parameters for laser powder bed fusion of Inconel 718", Proceedings of the 9th International Symposium on Superalloy 718 & Derivatives: Energy, Aerospace, and Industrial Applications, pp. 595–610, doi: 10.1007/978-3-319-89480-5_39

[13] Aoyagi, K., Wang, H., Sudo, H. and Chiba, A. (2019), "Simple method to construct process maps for additive manufacturing using a support vector machine", Additive Manufacturing, Vol. 27, pp. 353–362, doi: 10.1016/j.addma.2019.03.013.

[14] Rankouhi, B., Jahani, S., Pfefferkorn, F.E. and Thoma, D.J. (2021), "Compositional grading of a 316L-Cu multi-material part using machine learning for the determination of selective laser melting process parameters", Additive Manufacturing, Elsevier, Vol. 38, p. 101836, doi: 10.1016/j.addma.2021.101836

[15] Liu, Q., Wu, H., Paul, M.J., He, P., Peng, Z., Gludovatz, B., Kruzic, J.J., et al. (2020), "Machine-learning assisted laser powder bed fusion process optimization for AlSi10Mg: New microstructure description indices and fracture mechanisms", Acta Materialia, Elsevier, Vol. 201, pp. 316–328, doi: 10.1016/j.actamat.2020.10.010.

[16] Alamri, F., Barsoum, I., Bojanampati, S. and Maalouf, M. (2025), "Prediction of porosity, hardness and surface roughness in additive manufactured AlSi10Mg samples", PloS One, Public Library of Science San Francisco, CA USA, Vol. 20 No. 3, p. e0316600, doi: 10.1371/journal.pone.0316600.

[17] Miao, H., Yusof, F., Karim, M.S.A., Badruddin, I.A., Hussien, M., Kamangar, S. and

Zhang, H. (2023), “Process parameter optimisation for selective laser melting of AlSi10Mg-316L multi-materials using machine learning method”, The International Journal of Advanced Manufacturing Technology, Springer, Vol. 129 No. 7, pp. 3093–3108.

[18] Wang, R.-J., Li, J., Wang, F., Li, X. and Wu, Q. (2009), “ANN model for the prediction of density in selective laser sintering”, International Journal of Manufacturing Research, Inderscience Publishers, Vol. 4 No. 3, pp. 362–373, doi: 10.1504/IJMR.2009.026579

[19] Tapia, G., Elwany, A.H. and Sang, H. (2016), “Prediction of porosity in metal-based additive manufacturing using spatial Gaussian process models”, Additive Manufacturing, Elsevier, Vol. 12, pp. 282–290, doi: 10.1016/j.addma.2016.05.009

[20] Liu, Q., Chen, W., Yakubov, V., Kruzic, J.J., Wang, C.H. and Li, X. (2024), “Interpretable machine learning approach for exploring process-structure-property relationships in metal additive manufacturing”, Additive Manufacturing, Elsevier B.V., Vol. 85 No. February, p. 104187, doi: 10.1016/j.addma.2024.104187.

[21] Williams, C.K.I. and Rasmussen, C.E. (2006), Gaussian Processes for Machine Learning, Vol. 2, MIT press Cambridge, MA, doi: 10.1142/S0129065704001899

[22] Singh, A., Thakur, N., Sharma, A., Alamri, F., Barsoum, I., Bojanampati, S. and Maalouf, M. (2016), “A review of supervised machine learning algorithms”, 2016 3rd International Conference on Computing for Sustainable Global Development (INDIACom), Ieee, Vol. 20 No. 3, p. e0316600.

[23] Tolochko, N.K., Mozzharov, S.E., Yadroitsev, I.A., Laoui, T., Froyen, L., Titov, V.I. and Ignatiev, M.B. (2004), “Balling processes during selective laser treatment of powders”, Rapid Prototyping Journal, Emerald Group Publishing Limited, Vol. 10 No. 2, pp. 78–87, doi: 10.1108/13552540410526953

[24] Nudelis, N. and Mayr, P. (2022), “Defect-based analysis of the laser powder bed fusion process using X-ray data”, International Journal of Advanced Manufacturing Technology, Springer London, Vol. 123 No. 9–10, pp. 3223–3232, doi: 10.1007/s00170-022-10407-9.

[25] Yang, K. V, Rometsch, P., Jarvis, T., Rao, J., Cao, S., Davies, C. and Wu, X. (2018), “Porosity formation mechanisms and fatigue response in Al-Si-Mg alloys made by selective laser melting”, Materials Science and Engineering: A, Vol. 712, pp. 166–174, doi: 10.1016/j.msea.2017.11.078.

[26] Gu, D. and Shen, Y. (2009), "Balling phenomena in direct laser sintering of stainless steel powder: Metallurgical mechanisms and control methods", Materials & Design, Elsevier, Vol. 30 No. 8, pp. 2903–2910, doi: 10.1016/j.matdes.2009.01.013

[27] Li, R., Liu, J., Shi, Y., Wang, L. and Jiang, W. (2012), "Balling behavior of stainless steel and nickel powder during selective laser melting process", The International Journal of Advanced Manufacturing Technology, Springer, Vol. 59, pp. 1025–1035, doi: 10.1007/s00170-011-3566-1.

[28] Phutela, C., Bosio, F., Li, P. and Aboulkhair, N.T. (2023), "Correlating the microstructure and hardness of AlSi10Mg powder with additively-manufactured parts upon in-situ heat-treatments in laser beam powder bed fusion", Additive Manufacturing Letters, Elsevier B.V., Vol. 7 No. August, p. 100168, doi: 10.1016/j.addlet.2023.100168.

[29] Ashwath, P., Xavior, M.A., Batako, A., Jeyapandiarajan, P. and Joel, J. (2022), "Selective laser melting of Al–Si–10Mg alloy: microstructural studies and mechanical properties assessment", Journal of Materials Research and Technology, Vol. 17, pp. 2249–2258, doi: 10.1016/j.jmrt.2022.01.135.

[30] Lv, F., Shen, L., Liang, H., Xie, D., Wang, C. and Tian, Z. (2019), "Mechanical properties of AlSi10Mg alloy fabricated by laser melting deposition and improvements via heat treatment", Optik, Elsevier, Vol. 179 No. October 2018, pp. 8–18, doi: 10.1016/j.ijleo.2018.10.112.

[31] Toprak, İ.B. and Dogdu, N. (2024), "Multi-Objective Optimization Study on Production of AlSi10Mg Alloy by Laser Powder Bed Fusion", Applied Sciences (Switzerland), Vol. 14 No. 22, doi: 10.3390/app142210584.